Applied Surface Science 258 (2012) 3714–3722

Contents lists available at SciVerse ScienceDirect

Applied Surface Science

journal homepage: www.elsevier.com/locate/apsusc

The dehydrogenation of CH_4 on Rh(1 1 1), Rh(1 1 0) and Rh(1 0 0) surfaces: A density functional theory study

Baojun Wang*, Luzhi Song, Riguang Zhang

Key Laboratory of Coal Science and Technology of Ministry of Education and Shanxi Province, Taiyuan University of Technology, Taiyuan 030024, Shanxi, China

ARTICLE INFO

Article history:
Received 21 August 2011
Received in revised form 2 December 2011
Accepted 2 December 2011
Available online 13 December 2011

Keywords:
CH_4
Dehydrogenation
Rh surface
Density functional theory

ABSTRACT

CH_4 dehydrogenation on Rh(1 1 1), Rh(1 1 0) and Rh(1 0 0) surfaces has been investigated by using density functional theory (DFT) slab calculations. On the basis of energy analysis, the preferred adsorption sites of CH_x (x = 0–4) and H species on Rh(1 1 1), Rh(1 1 0) and Rh(1 0 0) surfaces are located, respectively. Then, the stable co-adsorption configurations of CH_x (x = 0–3) and H are obtained. Further, the kinetic results of CH_4 dehydrogenation show that on Rh(1 1 1) and Rh(1 0 0) surfaces, CH is the most abundant species for CH_4 dissociation; on Rh(1 1 0) surface, CH_2 is the most abundant species, our results suggest that Rh catalyst can resist the carbon deposition in the CH_4 dehydrogenation. Finally, results of thermodynamic and kinetic show that CH_4 dehydrogenation on Rh(1 0 0) surface is the most preferable reaction pathway in comparison with that on Rh(1 1 1) and Rh(1 1 0) surfaces.

1. Introduction

The dehydrogenation of CH_4 is an important part of the mechanism for acetic acid synthesis via a two step-wise CH_4–CO_2 reaction [1,2] and CH_4–CO_2 reforming reaction [3–11] on transition mental surface, which has been attracting great interest. The adsorption and dissociation of CH_x (x = 0–4) on transition metal surface have been studied extensively by experimentalists [1,2,12,13] and by theoreticians [14–27] because of their industrial and commercial importance. A common feature is that the best catalysts are the group VIII metals Co, Ni, Ru, Rh, Ir, etc. Among of them, since Rh can lead to lower carbon deposition in the reaction related to CH_4 [11], Rh has been shown to be one of the most effective catalysts in a variety of industrial catalytic processes. Therefore, a detailed investigation about the adsorption and dissociation of hydrocarbon species on Rh surface will be useful to gain some insights into understanding the corresponding catalytic processes. For example, the studies by Choi and Liu [28] have shown that Rh-based catalyst presented unique efficiency and selectivity in catalyzing ethanol synthesis from syngas, and Rh(1 1 1) is highly selective to CH_4 rather than ethanol. Horn et al. [29] have studied the Rh and Pt catalysts for the partial oxidation of CH_4 to syngas, and found that the selectivity and yield of H_2 and CO are higher in the oxidation zone on Rh than that on Pt.

Over the past decades, it has been demonstrated that theoretical techniques can serve as powerful tools for providing qualitative and quantitative insights into the structure of active surfaces and surface interaction [30–33]. Up to now, although several density functional theory (DFT) studies have been carried out on CH_4 dissociation, most of them were focused on metal cluster model, for example, the extensive studies by Liao and Zhang [22], Au et al. [23,24] and Kua et al. [34], involved Rh, Ir, Os, Ni, Pd, Pt and Cu metal cluster surfaces. However, it is generally accepted that cluster model has boundary effect due to dangling bonds. Meanwhile, Henkelman and Jónsson [35] demonstrated that the relaxations of metal surface greatly influenced the geometry and energy of transition state. Thus, the periodic slab models are much better suited for this type of calculation. Up to now, many theoretical studies have been carried out to investigate the adsorption of CH_x on Ru(1 1 −2 0) [6], Ru(0 0 0 1) [27], Pd(1 1 1) [10], and CH_4 dehydrogenation on Ru(0 0 0 1) [14,15], Co(1 1 1) [8], Ni(1 1 1) [3–9,36–40], Ni(1 0 0) [8,37,40] and Ir(1 1 1) [13], in which the periodic slab models are used. For CH_4 dehydrogenation on Rh(1 1 1), Rh(1 1 0) and Rh(1 0 0) surfaces, only Bunnik and Kramer [17] investigated the dissociation of CH_4 on Rh(1 1 1) surface by using DFT method together with periodic slab models, which presented the most stable adsorption sites of CH_x, and found that the activation barrier of CH dehydrogenation is the highest. Kokalj et al. [20,21] studied the first two dehydrogenation of CH_4 on Rh(1 1 1) and Rh@Cu(1 1 1) surface, respectively. Above reported studies show that even though Rh is an important

* Corresponding author at: No. 79 Yingze West Street, Taiyuan 030024, China. Tel.: +86 351 6018539; fax: +86 351 6041237.
E-mail address: wangbaojun@tyut.edu.cn (B. Wang).

0169-4332/$ – see front matter © 2011 Elsevier B.V. All rights reserved.
doi:10.1016/j.apsusc.2011.12.012

catalyst candidate, the interaction of CH_4 with Rh catalyst is seldom reported, only with Rh(1 1 1) surface [17,19,28,41–48].

Therefore, in this study, DFT calculations are performed to systematically investigate the adsorption of CH_4 and its dissociation products, CH_x and H, on Rh(1 1 1), Rh(1 1 0) and Rh(1 0 0) surfaces, to elucidate the preferred adsorption site and dehydrogenation mechanism of CH_4, as well as to understand the microscopic reasons of resisting carbon deposition on Rh catalyst behind the reaction, which may be of interest to researchers attempting to illustrate the catalytic mechanism involving in CH_4 reaction on Rh catalyst. This paper is organized as follows: in Section 2, we provide a detailed calculation models and methods, in Section 3, we present our comparative investigations of CH_x (x = 0–4) and H adsorption on Rh(1 1 1), Rh(1 1 0) and Rh(1 0 0) surfaces; then, the co-adsorption of CH_x (x = 0–3) and H on Rh(1 1 1), Rh(1 1 0) and Rh(1 0 0) surfaces; finally, we discuss the dehydrogenation mechanism of CH_4. The conclusions are presented in the final section.

2. Computational models and methods

2.1. Surface models

Based on the optimized Rh bulk structure, the four-layered Rh(1 1 1), Rh(1 1 0) and Rh(1 0 0) surfaces model were built, and a p(2 × 2) super-cell is employed (16 Rh atoms in a cell), which has been widely used in the previous theoretical studies about molecule interaction with metal surface [41,42,48]. Further, a p(2 × 3) surface super-cell has also been considered to obtain the size effect of surface on calculation, which suggest that a p(2 × 2) super-cell is large enough to neglect the lateral adsorbate interactions. Therefore, taking the calculation efficiency into consideration, a p(2 × 2) super-cell is employed in our study, as shown in Fig. 1. For Rh(1 0 0) surface, there are three adsorption sites: top (T), bridge (B), hollow (H); for Rh(1 1 0) surface: top (T), short bridge (SB), long bridge (LB), hollow (H); for Rh(1 1 1) surface: top (T), bridge (B), fcc, hcp. The vacuum space of 10 Å is inserted in the direction perpendicular to the surface in order to prevent interactions between periodic images. In all calculations, Rh atoms of the top three layers and adsorbed species are allowed to relax, while those in other layers are fixed. In addition, in order to differentiate top- and second-layer of the slab, the second-layer have been marked in dark-orange balls.

2.2. Calculation methods

In this study, DFT has been employed to perform for all calculation with the program Cambridge Sequential Total Energy Package (CASTEP) [49] in the Materials studio 4.4 of Accelry Inc. The exchange and correlation energies are employed using the Perdew-Wang-91 (PW91) functional within the generalized gradient approximation (GGA) [50,51], combined with Vanderbilt ultra-soft pseudopotentials [52]. A plane wave cut-off energy of 310 eV [53,54] is used. The meshes are set to k-points 5 × 5 × 1 for Rh(1 1 1), 3 × 5 × 2 for Rh(1 1 0) and 5 × 5 × 2 for Rh(1 0 0) surface. The convergence criteria are set to the tolerance for SCF, energy, maximum force, and maximum displacement of 2.0×10^{-6} eV/atom, 2.0×10^{-5} eV/atom, 0.05 eV/Å and 2.0×10^{-3} Å, respectively. Moreover, the transition states (TS) are searched by means of complete LST/QST method for reactions [55], starting from reactants and products, the LST (Linear Synchronous Transit) method performs a single interpolation to a maximum energy, and the QST (Quadratic Synchronous Transit) method alternates searches for an energy maximum with constrained minimizations in order to refine the transition state to a high degree. In addition, since CASTEP program cannot obtain the frequency information, Dmol^3 program is employed to calculate the frequency of transition state with the same calculation methods.

The adsorption energy is defined as follows:

$$E_{ads} = E_{adsorbate} + E_{slab} - E_{adsorbate/slab}$$

where $E_{adsorbate/slab}$ is the total energy of the slab together with the adsorbate, $E_{adsorbate}$ is the total energy of the free adsorbate, and E_{slab} is the total energy of the bare slab. With this definition, positive values of adsorption energy denote that adsorption is more stable than the corresponding slab and free adsorbate.

3. Results and discussion

3.1. Calculation of CH_4 molecule and bulk Rh

The obtained values verify the credibility of the selected calculation methods: firstly, the bond length and bond angle of CH_4 calculated from our approach are $r_{(C-H)}$ = 1.096 Å and $\theta_{(H-C-H)}$ = 109.5°, respectively, which are in good agreement with the experimental values of 1.096 Å, 109.4° [56], respectively. Then, the next test is to predict the lattice constant of bulk Rh. The calculated value for the lattice constant is 3.902 Å, which is close to the experimental value of 3.803 Å [57], as well as with other similar GGA results [28,58]. Such results obtained in these tests make us confident in this study.

To investigate the mechanism of CH_4 dehydrogenation on Rh(1 1 1), Rh(1 1 0) and Rh(1 0 0) surfaces, we need to know the individual bonding natures of different species, for example, CH_x

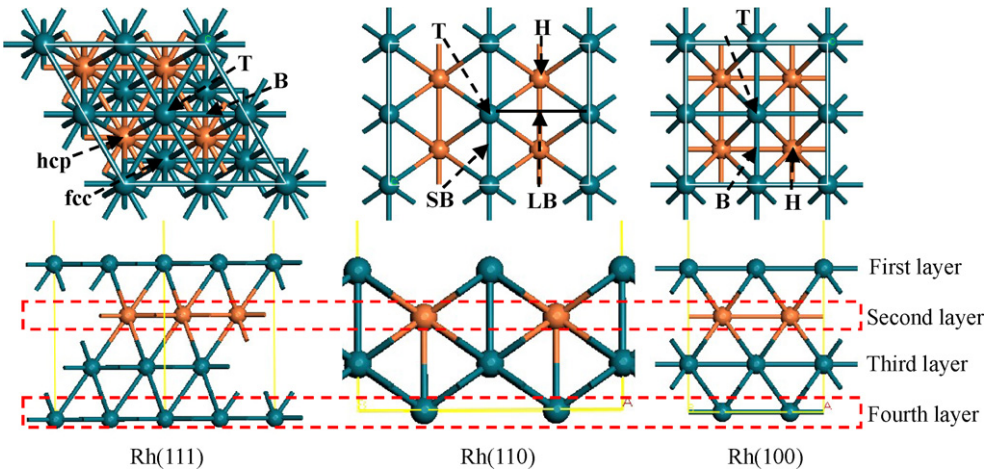

Fig. 1. Top view of Rh(1 1 1), Rh(1 1 0) and Rh(1 0 0). Top site – T; bridge site – B; hollow site – H; short bridge – SB; long bridge – LB.

(x = 0–4) and H species adsorbed on Rh(1 1 1), Rh(1 1 0) and Rh(1 0 0) surfaces, different adsorption sites on Rh(1 1 1), Rh(1 1 0) and Rh(1 0 0) surfaces are considered. So we will first investigate the stability of H and CH_x (x = 0–4) species at all adsorption sites, then, we will discuss the co-adsorption of CH_x (x = 0–3) and H atom on Rh(1 1 1), Rh(1 1 0) and Rh(1 0 0) surfaces. After that, we probe into the dehydrogenation mechanism of CH_4 to the final products C and H, in which every elementary reaction will be analyzed.

3.2. Adsorbed CH_x (x = 0–4) and H on Rh(1 1 1), Rh(1 1 0) and Rh(1 0 0) surfaces

3.2.1. Adsorbed CH_x and H on Rh(1 1 1) surface

Adsorbed CH_4. According to the surface morphology, several orientations of the CH_4 molecule are examined at different sites. It is generally accepted that CH_4 orientation with respect to Rh(1 1 1) surface is not a determinative parameter, so we only study one H of CH_4 point toward the surface before geometrical optimization [7–9,59]. Four stable structures are found, CH_4 (T), CH_4 (B), CH_4 (fcc) and CH_4 (hcp), and the corresponding adsorption energies are 12.1, 9.7, 10.5 and 10.5 kJ mol^{-1}, respectively, which indicate that CH_4 prefers to adsorb at the top site of Rh(1 1 1) surface, as shown in Fig. 2(a). We can see that the Rh–H distance is 2.249 Å for the case of adsorbed CH_4 with one H atom pointing down to the surface, and CH_4 molecule is not distorted.

Adsorbed CH_3. Four stable structures are also obtained, the corresponding adsorption energies are 247.8, 250.0, 257.8 and 255.3 kJ mol^{-1} for CH_3 (T), CH_3 (B), CH_3 (fcc) and CH_3 (hcp), respectively, which is consistent with the earlier calculations on Rh(1 1 1) [41,60,61]. It indicates that CH_3 prefers to adsorb at the fcc site (see Fig. 2(b)), the C—Rh bond lengths are 2.277, 2.284 and 2.289 Å, and one C—H bond length is (1.122 Å) is larger than that (1.086 Å) of free CH_3.

Adsorbed CH_2. CH_2 prefers to adsorb at the hcp site (see Fig. 2(c)), and the adsorption energy is 473.4 kJ mol^{-1}. At the top and fcc sites, the corresponding adsorption energies are 397.4 and 469.2 kJ mol^{-1}, respectively. The initial structure at the bridge site is optimized into that at the hcp site. The C—H bond lengths are 1.119 and 1.124 Å, respectively. The angle of H—C—H is 106.4° for hcp adsorption mode, the C—Rh bond lengths are 2.024, 2.152 and 2.164 Å, respectively.

Adsorbed CH. CH prefers to adsorb at the hcp site (see Fig. 2(d)), the adsorption energy is 704.0 kJ mol^{-1}. At the fcc site, the adsorption energy is 683.5 kJ mol^{-1}. The initial structures at the top and bridge sites are optimized into those at the fcc and hcp sites, respectively. The C—H bond length is shorten to 1.103 Å from that of free CH (1.136 Å), and the C—Rh bond lengths are 2.002, 2.005 and 2.006 Å at the hcp site.

Adsorbed C. Three stable structures are obtained for C. C prefers to adsorb at the hcp site (see Fig. 2(e)), and the adsorption energy is 825.0 kJ mol^{-1}, C interacts with three Rh atoms leading to the formation of three Rh—C bonds, all C—Rh bond lengths are 1.929 Å. At the top and fcc sites, the corresponding adsorption energy are 631.6 and 800.9 kJ mol^{-1}, respectively. The initial structure at the bridge site is optimized into that at the hcp site.

Adsorbed H. H adsorbs on Rh(1 1 1) surface have three stable structures, the initial structure at the bridge site is optimized into that at the fcc site. The corresponding adsorption energies are 352.7, 393.6 and 388.1 kJ mol^{-1} at the top, fcc and hcp sites, respectively, which suggests that H prefers to adsorb at the fcc site, as shown in Fig. 2(f), the C—Rh bond lengths are 1.881, 1.881 and 1.883 Å.

On the basis of above results, we can see that CH_4 adsorbed at four sites of Rh(1 1 1) surface is typical of physisorption. However,

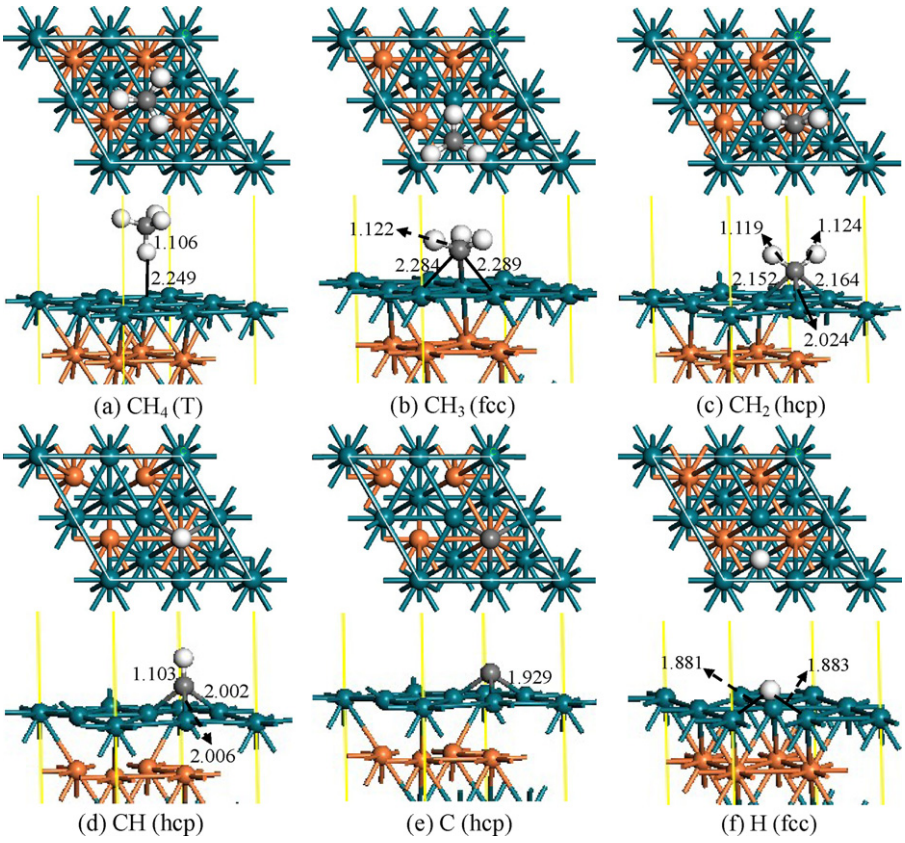

Fig. 2. Top and side view of the most stable configurations of CH_x and H adsorbed on Rh(1 1 1) surface. White balls: H, gray balls: C, green balls: Rh, dark-orange balls: Rh. Bond length unit is in Å. (For interpretation of the references to color in this figure legend and in text, the reader is referred to the web version of this article.)

CH_x (x = 0–3) and H species adsorbed on Rh(1 1 1) surface is strong chemisorption, in which CH_3 and H prefer to adsorb at the fcc sites, CH_2, CH and C prefer to adsorb at the hcp sites. Zuo et al. [8] reported that on Co(1 1 1) surface, CH_3 and H prefer to adsorb at the 3-fold hollow hcp and fcc sites, and CH_2, CH and C prefer to adsorb at the hcp sites. The studies by Wang et al. [9] showed that on Ni(1 1 1) surface, CH_3, CH_2 and H prefer to adsorb at the 3-fold hollow hcp and fcc sites, at the same time, hcp site is the most stable one for C and CH.

3.2.2. Adsorbed CH_x and H on Rh(1 1 0) surface

The most stable adsorption configuration of CH_x and H species on Rh(1 1 0) surface with the key geometrical parameters are presented in Fig. 3. As shown in Fig. 3, for CH_4 adsorption, CH_4 adsorbed at the top site is the most stable configuration (see Fig. 3(a)), in which CH_4 molecule is not distorted. The Rh–H distance is 2.173 Å, and the adsorption energy is 60.4 kJ mol^{-1}. CH_3 prefers to the SB site, as shown in Fig. 3(b), and the adsorption energy is 321.6 kJ mol^{-1}. The C—Rh bond lengths are 2.101 and 2.297 Å, respectively. For CH_2 adsorption, CH_2 adsorbs at the LB site (see Fig. 3(c)), in which the C—Rh bond lengths are 2.035 and 2.036 Å, respectively, and the adsorption energy is 538.1 kJ mol^{-1}. CH prefers to the LB site, as presented in Fig. 3(d), the adsorption energy is 733.5 kJ mol^{-1}, and the C—Rh bond lengths are 2.080 and 2.082 Å. For C atom adsorption, C also prefers to adsorb at the LB site (see Fig. 3(e)), the adsorption energy is 912.1 kJ mol^{-1}, and the C—Rh bond lengths are 1.980 and 1.983 Å, respectively. Finally, H adsorbed at the SB site is the most stable configuration, as shown in Fig. 3(f), the corresponding adsorption energy is 420.9 kJ mol^{-1}, and both H—Rh bond lengths are 1.764 Å.

3.2.3. Adsorbed CH_x and H on Rh(1 0 0) surface

The most stable adsorption configuration of CH_x and H species on Rh(1 0 0) surface with the key geometrical parameters are presented in Fig. 4. As shown in Fig. 4, for CH_4 adsorption, the initial structure at the hollow site is optimized into that at the bridge site. CH_4 adsorbed at the top site (see Fig. 4(a)) is the most stable configuration with the adsorption energy of 15.9 kJ mol^{-1}, and CH_4 molecule is still not distorted. CH_3 prefers to adsorb at the bridge site, as shown in Fig. 4(b), the corresponding adsorption energy is 265.4 kJ mol^{-1}, the C—Rh bond lengths are 2.194 and 2.200 Å, respectively. For CH_2 adsorption, CH_2 prefers to adsorb at the hollow site (see Fig. 4(c)), the adsorption energy is 514.7 kJ mol^{-1}. The C—H bond lengths are 1.105 and 1.260 Å, respectively, and H—C—H bond angle is 109.1° at the hollow site. CH also prefers to adsorb the hollow site, as presented in Fig. 4(d), the adsorption energy is 755.6 kJ mol^{-1}. The C—H bond length is 1.112 Å, and all the C—Rh bond lengths are 2.119 Å at the hollow site. C adsorbed at the hollow site is the most stable configuration (see Fig. 4(e)), the initial structure at the bridge site is optimized into that at the hollow site, and the adsorption energy is 924.4 kJ mol^{-1}, all the C—Rh bond length are 2.014 Å at the hollow site. For H adsorption, H adsorbed at the bridge site is the most stable configuration with the adsorption energy of 393.3 kJ mol^{-1}, as shown in Fig. 4(f), the H—Rh bond lengths are 1.768 and 1.768 Å.

Therefore, above results about CH_x (x = 0–4) and H adsorbed on Rh(1 1 1), Rh(1 1 0) and Rh(1 0 0) surfaces show that despite of the discrepancies among the various studies in the precise values for the adsorption energies, these investigations can conclude the general trend in the adsorption energies: $CH_4 < CH_3 < H < CH_2 < CH < C$. Our calculated results are in agreement with the reported results [8,10,14,18,27,42].

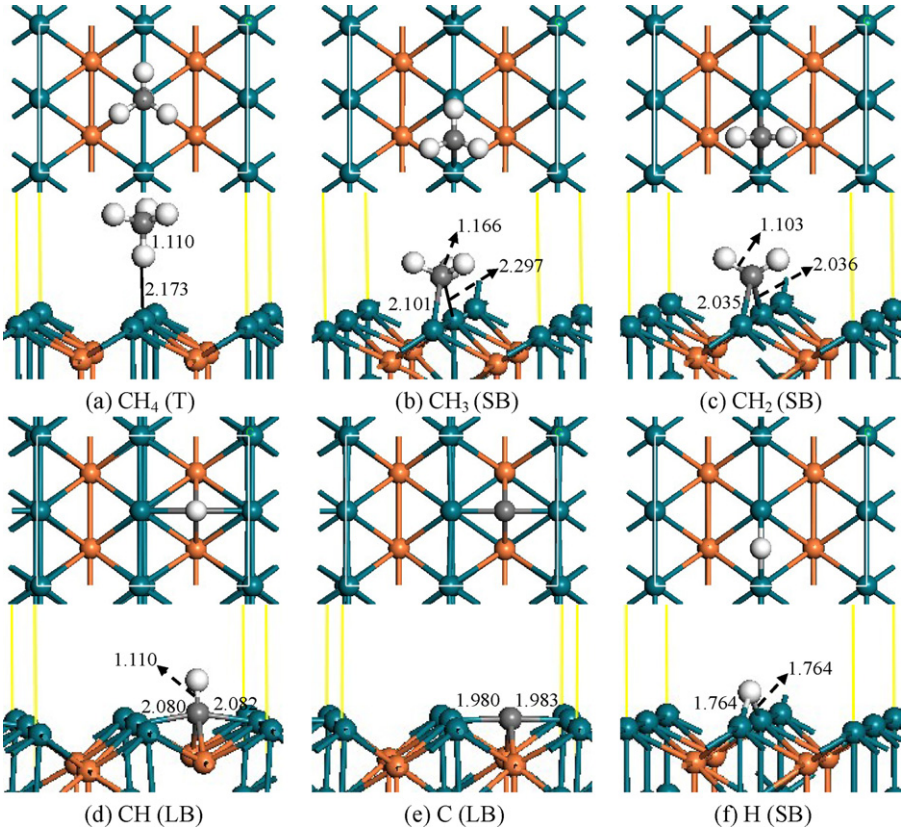

Fig. 3. Top and side view of the most stable configurations of CH_x and H adsorbed on Rh(1 1 0) surface.

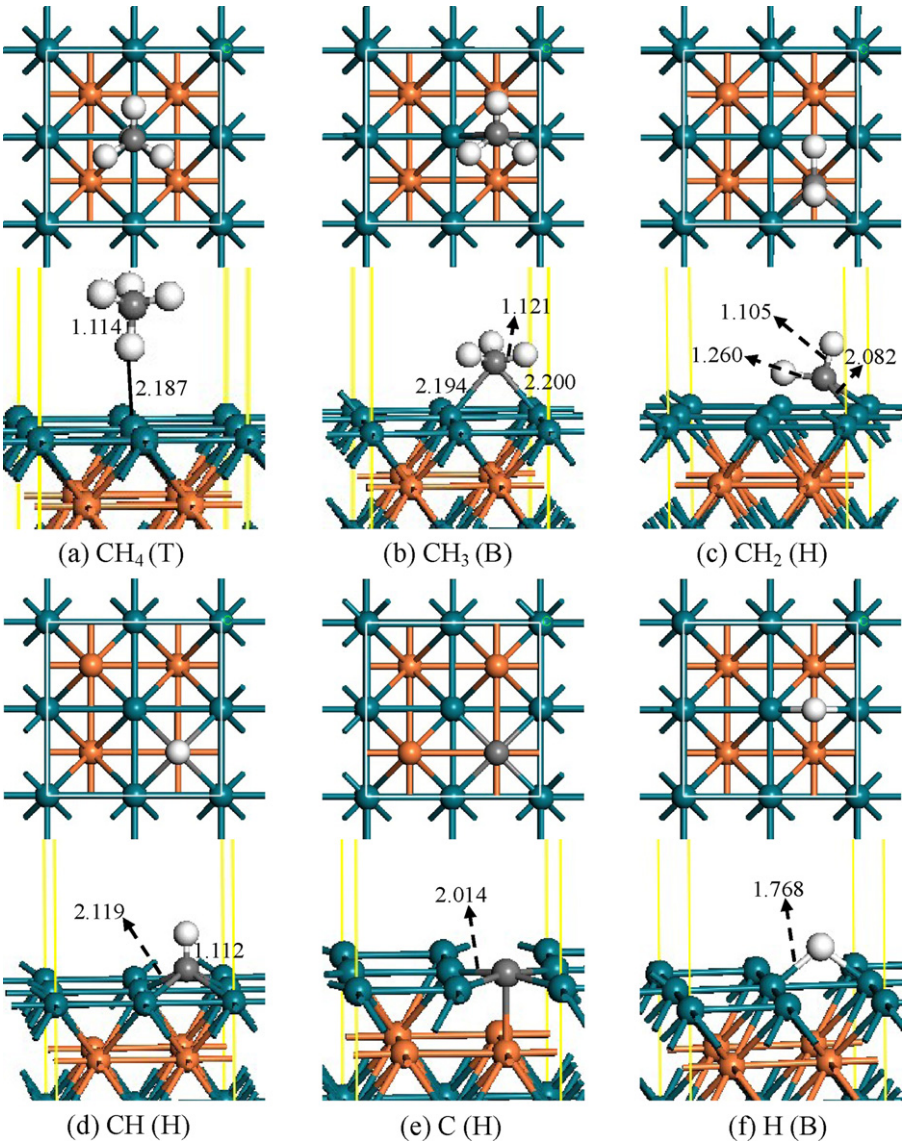

Fig. 4. Top and side view of the most stable configurations of CH_x and H adsorbed on Rh(1 0 0) surface.

3.3. *The co-adsorption of CH_x (x = 0–3) and H on Rh(1 1 1), Rh(1 1 0) and Rh(1 0 0) surfaces*

The co-adsorption energy of CH_x and H on Rh(1 1 1), Rh(1 1 0) and Rh(1 0 0) surfaces can be defined as follows:

$$E_{\text{co-ads}} = E(\text{A}) + E(\text{B}) + E(\text{slab}) - E((\text{A}+\text{B})/\text{slab})$$

where E(A), E(B), E(slab) and E((A + B)/slab) are the total energy for the free molecule A and B, the slab with a (2×2) supercell and the co-adsorbed (A + B)/slab systems, respectively.

In all calculations, for the most stable co-adsorption configuration of CH_x (x = 0–3) and H on Rh(1 1 1), Rh(1 1 0) and Rh(1 0 0) surfaces, we consider that CH_x (x = 0–3) and H are respectively

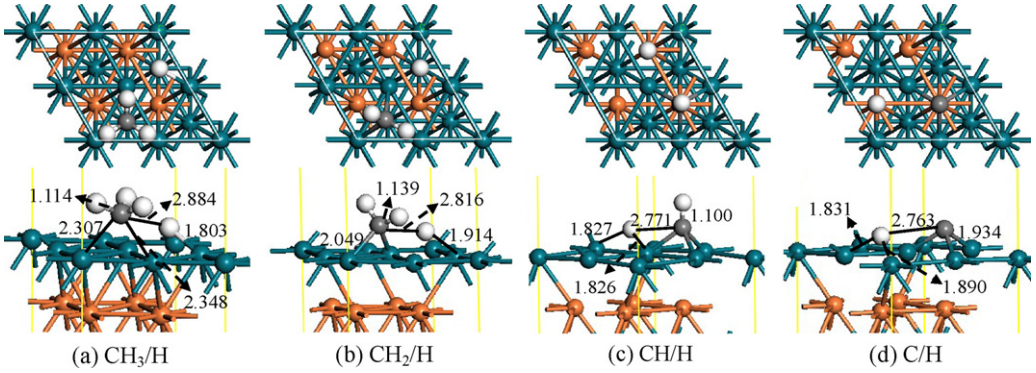

Fig. 5. Top and side view of the optimized structures of the co-adsorbed CH_x + H on Rh(1 1 1).

Table 1
The co-adsorption energies (kJ mol^{-1}) and the adsorption sites in the stable co-adsorption configuration of CH_x and H on Rh(1 1 1), Rh(1 1 0) and Rh(1 0 0) surfaces.

Surface	CH_3/H		CH_2/H		CH/H		C/H	
	Model	$E_{co\text{-}ads}$	Model	$E_{co\text{-}ads}$	Model	$E_{co\text{-}ads}$	Model	$E_{co\text{-}ads}$
Rh(1 1 1)	fcc–fcc	627.3	B–fcc	860.5	hcp–hcp	1077.8	hcp–hcp	1186.9
Rh(1 1 0)	SB–SB	694.9	SB–SB	925.4	LB–SB	1104.0	LB–SB	1286.0
Rh(1 0 0)	B–B[a]	652.6	B–B	871.9	H–H	1141.5	H–H	1303.7

[a] B–B denotes that on Rh(1 0 0) surface, CH_3 and H are adsorbed at the adjacent bridge site in the optimized stable co-adsorption configuration of CH_3 and H. Other models are the same meanings.

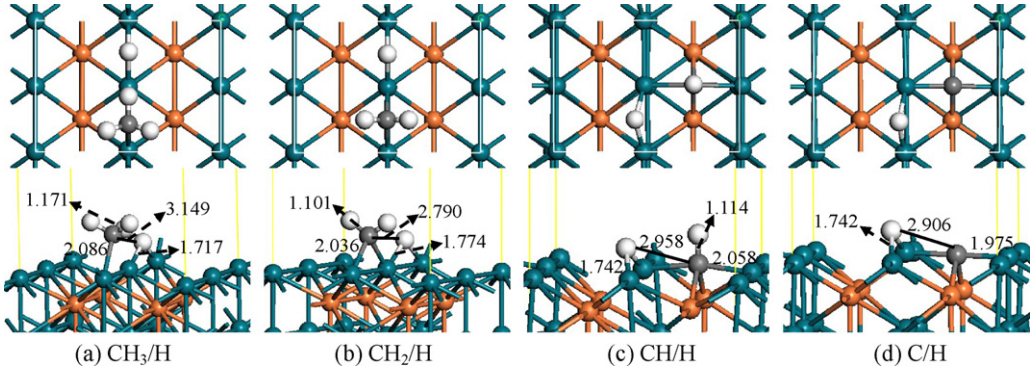

Fig. 6. Top and side view of the optimized structures of the co-adsorbed CH_x + H on Rh(1 1 0).

placed at the adjacent and the most stable adsorption sites. For example, for the most stable co-adsorption configuration of CH_3 and H on Rh(1 1 1) surface, it has been pointed out that the CH_3 and H placed at the fcc sites is the most stable configuration. Hence, in the initial co-adsorption configuration of CH_3 and H, CH_3 and H are placed at the adjacent fcc site on Rh(1 1 1) surface, the optimized co-adsorption configuration is shown in Fig. 5(a), and the co-adsorption energy is 627.3 kJ mol^{-1}, in which the distance of H and CH_3 is 2.884 Å. Then, the stable co-adsorption configuration of CH_2 and H are presented in Fig. 5(b), in which CH_2 and H are located at the adjacent bridge and fcc site, respectively, and the co-adsorption energy is 860.5 kJ mol^{-1}, the distance of H—CH_2 is 2.816 Å. Afterwards, Fig. 5(c) gives the stable co-adsorption configuration of CH and H, in which CH and H site are located at the adjacent hcp sites, and the co-adsorption energy is 1077.8 kJ mol^{-1}, the distance of H—CH is 2.771 Å. Finally, the stable co-adsorption configuration of C and H are shown in Fig. 5(d), in which C and H are adsorbed at the adjacent hcp sites, and the co-adsorption energy is 1186.9 kJ mol^{-1}, the distance of H—C is 2.763 Å. As a result, the co-adsorption energies and the adsorption sites in the stable co-adsorption configuration of CH_x and H on Rh(1 1 1), Rh(1 1 0) and Rh(1 0 0) surfaces are listed in Table 1, and the stable configurations of CH_x and H with key structural parameters are presented in Figs. 5–7.

3.4. CH_4 dehydrogenation on Rh(1 1 1), Rh(1 1 0) and Rh(1 0 0) surfaces

After obtaining the most stable co-adsorption configuration of CH_x (x = 0–3) and H species, CH_3/H, CH_2/H, CH/H, C/H, we can calculate the elementary step of CH_4 sequence dehydrogenation on Rh(1 1 1), Rh(1 1 0) and Rh(1 0 0) surfaces. For CH_4 dehydrogenation on transition metal surfaces, the first step is dehydrogenation of CH_4 to CH_3. Hence, the most stable CH_4 configuration is

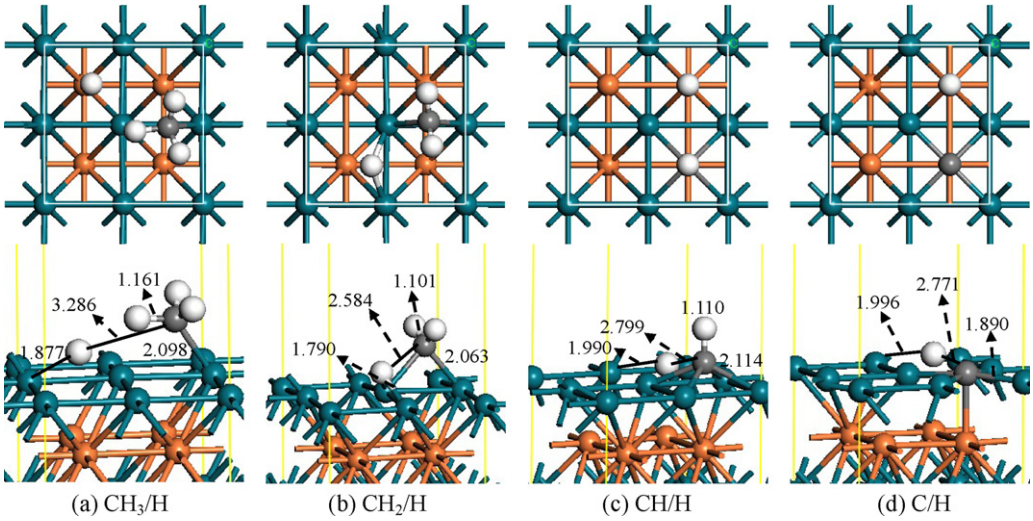

Fig. 7. Top and side view of the optimized structures of the co-adsorbed CH_x + H on Rh(1 0 0).

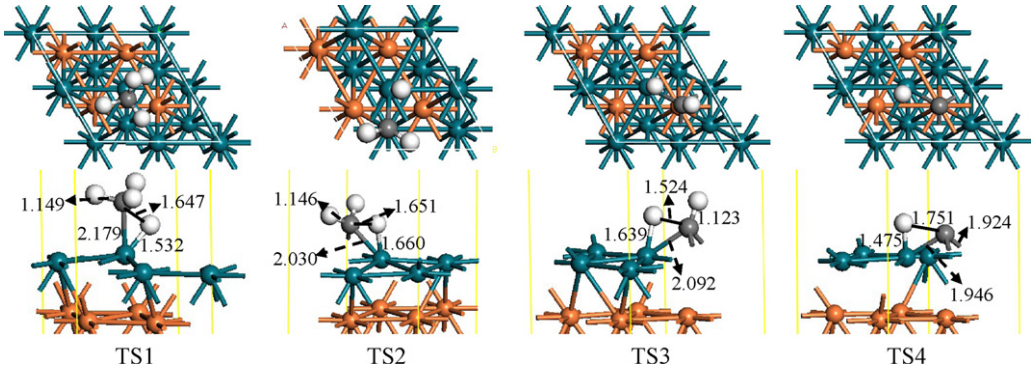

Fig. 8. Top and side view of the TS structures for CH_4 dehydrogenation on Rh(1 1 1).

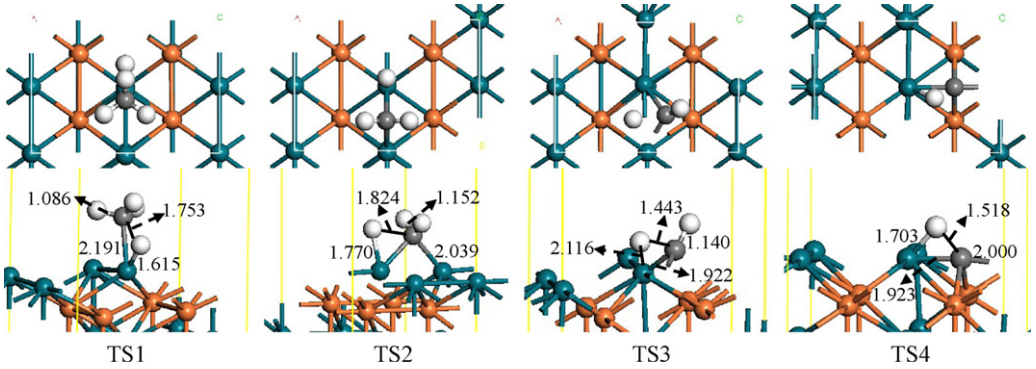

Fig. 9. Top and side view of the TS structures for CH_4 dehydrogenation on Rh(1 1 0).

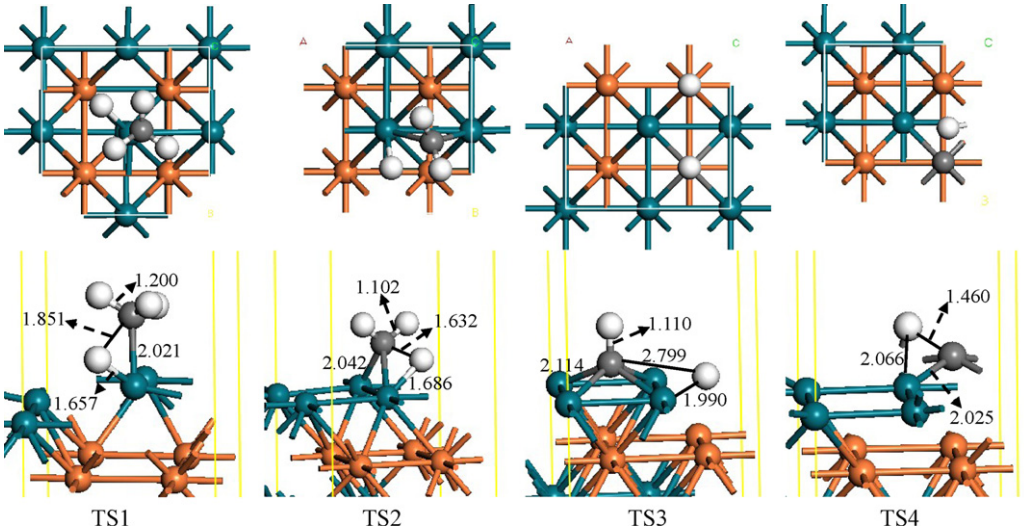

Fig. 10. Top and side view of the TS structures for CH_4 dehydrogenation on Rh(1 0 0).

chosen to be the initial state, and the final state consists of the stable co-adsorption configuration of CH_3 and H. The activation barriers and reaction energies of the most favored step are given out in this study, and the energy profile for the dehydrogenation of CH_4 on Rh(1 1 1), Rh(1 1 0) and Rh(1 0 0) surfaces is shown in Fig. 11, which illustrates the energy change for the whole process of CH_4 dehydrogenation from CH_4 to C.

In order to validate the structure of the transition state, the frequency analysis of transition state (TS) for CH_4 dehydrogenation on Rh(1 1 1), Rh(1 1 0) and Rh(1 0 0) surfaces have been examined, as listed in Table 2, the corresponding TS structures are shown in Figs. 8–10. It is noted that TS1 in Table 2 is the transition state of

Table 2
The imaginary frequency of transition states for CH_4 dehydrogenation on Rh(1 1 1), Rh(1 1 0) and Rh(1 0 0) surfaces.

Surface	Imaginary frequency (cm^{-1})			
	TS1	TS2	TS3	TS4
Rh(1 1 1)	−908.2	−897.1	−764.9	−892.8
Rh(1 1 0)	−891.8	−480.6	−849.9	−969.4
Rh(1 0 0)	−507.3	−706.9	−421.6	−832.5

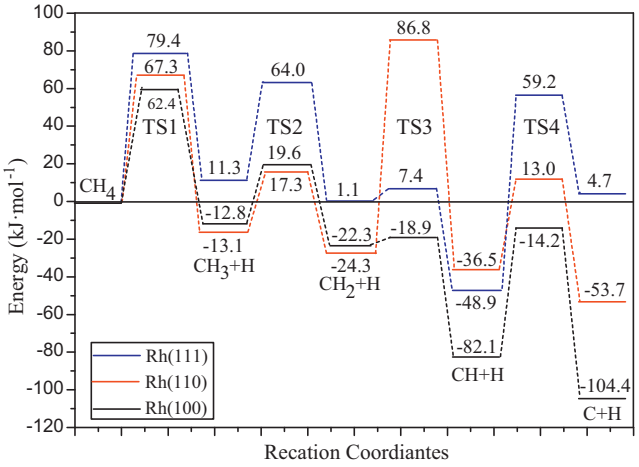

Fig. 11. The energy profiles of the CH_4 dehydrogenation to C on Rh(1 1 1), Rh(1 1 0) and Rh(1 0 0) surfaces.

CH_4 dehydrogenation into CH_3 and H, TS2 is the transition state of CH_3 dehydrogenation into CH_2 and H, TS3 is that of CH_2 dehydrogenation into CH and H, TS4 is that of CH dehydrogenates into C and H. We can see from Table 2 that every transition state has only one imaginary frequency. In addition, TS confirmation is performed on every transition state structure to confirm that they lead to the desired reactants and products.

As shown in Fig. 11, on Rh(1 1 1) surface, CH_4 dehydrogenates into CH_3 and H, which needs to overcome an activation barrier of 79.4 kJ mol^{-1}, and that of back reaction is 68.1 kJ mol^{-1}. The activation barrier of CH_3 dehydrogenation into CH_2 and H is 52.7 kJ mol^{-1}, and that of its back reaction barrier is 62.9 kJ mol^{-1}. CH_2 dehydrogenation into CH and H needs to overcome an activation barrier of 6.3 kJ mol^{-1}, and that of its back reaction barrier is 56.3 kJ mol^{-1}, which suggest that when CH_2 dissociates into CH and H, CH and H is very hard to form CH_2. Further, dehydrogenation of CH to C and H needs to overcome a very large activation barrier of 108.1 kJ mol^{-1}, and its back reaction barrier is 54.5 kJ mol^{-1}, which show that CH dissociating into C and H is a strong endothermic process. The high barriers and the strong endothermicity indicate that CH dehydrogenation on Rh(1 1 1) surface is unfavorable both kinetically and thermodynamically. The activation barrier is consistent with the results by Bunnik and Kramer [17] and Kokalj et al. [21]. Therefore, CH is the most abundant species on Rh(1 1 1) surface, which means that CH_4 dehydrogenation on Rh(1 1 1) surface can resist carbon deposition.

On Rh(1 1 0) surface, CH_4 dehydrogenates into CH_3 and H, which needs to overcome an activation barrier of 67.3 kJ mol^{-1}, and that of back reaction is 80.4 kJ mol^{-1}. Subsequently, the activation barrier of CH_3 dehydrogenation into CH_2 and H is 30.4 kJ mol^{-1}, and that of its back reaction is 41.6 kJ mol^{-1}. Compared to CH_4 dehydrogenation, CH_3 dehydrogenation into CH_2 and H is much easier. Then, the dehydrogenation of CH_2 to CH and H needs to overcome an activation barriers of 111.1 kJ mol^{-1}, and that of CH_2 hydrogenation to CH_3 is 123.3 kJ mol^{-1}. Further, dehydrogenation of CH to C and H needs to overcome an activation barrier of 49.5 kJ mol^{-1}, and its back reaction barrier is 66.7 kJ mol^{-1}. Above results show that CH_2 is very difficult to dissociate into CH and H, while CH_3 dehydrogenation into CH_2 and H is a kinetically favored step. Thus, we think that CH_2 is the most abundant species on Rh(1 1 0) surface, which suggest that CH_4 dehydrogenation on Rh(1 1 0) surface can also resist carbon deposition.

On Rh(1 0 0) surface, CH_4 dehydrogenates into CH_3 and H, which needs to overcome an activation barrier of 62.4 kJ mol^{-1}, and that of back reaction is 75.2 kJ mol^{-1}. Then, the activation barrier of CH_3 dehydrogenation into CH_2 and H is 32.4 kJ mol^{-1}, and that of its back reaction barrier is 41.9 kJ mol^{-1}. Further, the dehydrogenation of CH_2 to CH and H needs to overcome an activation barrier of 3.4 kJ mol^{-1}, and that of CH_2 hydrogenation to CH_3 is 63.2 kJ mol^{-1}. Finally, dehydrogenation of CH to C and H needs to overcome a barrier of 67.9 kJ mol^{-1}, and its back reaction barrier is 90.2 kJ mol^{-1}, suggesting that it is very difficult for CH dehydrogenation into C and H, while CH_2 dehydrogenation into CH and H is the most kinetically favored step. Hence, CH is the most abundant species on Rh(1 0 0) surface, and CH_4 dehydrogenation on Rh(1 0 0) surface can still resist carbon deposition.

Koster and Santen [62] have studied the dissociation of CO on the (1 1 1), stepped (1 1 1), (1 1 0), (1 0 0) surfaces of Rh, it is found that the activation barriers are lowest for Rh(1 0 0), and higher for Rh(1 1 0) and Rh(1 1 1). In addition, Hopstaken and Niemantsverdriet [63] have investigated the dissociation and desorption of NO on the (1 0 0) surface of Rh, it appears that the dissociation of NO proceeds faster on the more open Rh(1 0 0) surface, compared with earlier studies on Rh(1 1 1). Therefore, we think that CH_4 dehydrogenation on Rh(1 0 0) surface should be the most probable reaction pathway on the basis of its lowest activation energy in comparison with those on Rh(1 1 0) and Rh(1 1 1) surfaces.

3.5. The rate constants for CH_4 dehydrogenation

To further understand the reaction mechanism of CH_4 dehydrogenation on Rh(1 1 1), Rh(1 1 0) and Rh(1 0 0) surfaces at different temperature from the kinetic point of view, we calculated the rate constants in the temperature range of 298.15–1000 K, as listed in Table 3. The rate constants for these reaction pathways have been obtained using Eyring's transition state theory (TST) [64].

Table 3
The rate constant k (s^{-1}) for CH_4 dehydrogenation at different temperature on Rh(1 1 1), Rh(1 1 0) and Rh(1 0 0) surfaces.

Surface	Temperature (K)	Rate constant k (s^{-1})			
		CH_4—CH_3 + H	CH_3—CH_2 + H	CH_2—CH + H	CH—C + H
Rh(1 1 1)	298.15	6.73×10^{-1}	1.45×10^{6}	5.15×10^{11}	5.08×10^{-5}
	500	2.01×10^{5}	1.17×10^{9}	9.45×10^{11}	5.33×10^{2}
	700	6.13×10^{7}	2.14×10^{10}	1.38×10^{12}	4.67×10^{5}
	1000	6.47×10^{9}	2.02×10^{11}	2.1×10^{12}	7.04×10^{7}
Rh(1 1 0)	298.15	2.77×10^{3}	7.53×10^{8}	1.07×10^{-4}	2.87×10^{6}
	500	3.26×10^{7}	1.39×10^{10}	2.85×10^{2}	3.99×10^{9}
	700	2.15×10^{9}	5.28×10^{10}	1.23×10^{5}	9.92×10^{10}
	1000	6.04×10^{10}	1.56×10^{11}	1.02×10^{7}	1.28×10^{12}
Rh(1 0 0)	298.15	1.00×10^{4}	1.12×10^{8}	1.93×10^{15}	2.99×10^{2}
	500	9.23×10^{6}	1.07×10^{10}	1.01×10^{14}	5.34×10^{6}
	700	6.26×10^{8}	8.97×10^{10}	2.47×10^{13}	4.04×10^{8}
	1000	2.17×10^{10}	5.23×10^{11}	6.98×10^{12}	1.23×10^{10}

From Table 3, we can see that the rate constant k increases rapidly with the temperature increasing, but the increasing extent becomes small when the temperature is higher. At the same temperature, on Rh(1 1 1) and Rh(1 0 0) surfaces, the rate constant of CH dehydrogenation into C and H is the smallest than that of other pathways, and this sequence does not change with the temperature change, which implies that CH dehydrogenation into C and H is the rate-determining step. On Rh(1 1 0), the rate constant of CH_2 dehydrogenation into CH and H is the smallest, which implies that CH_2 dehydrogenation into CH and H is the rate-determining step.

On the basis of the above analysis of activation barriers and rate constants, we can obtain that, on Rh(1 1 1) and Rh(1 0 0) surfaces, CH dehydrogenation is the rate-determining step; on Rh(1 1 0) surface, CH_2 dehydrogenation is the rate-determining step of CH_4 dissociation. That is to say, CH and CH_2 is the most abundant CH_x species of CH_4 dehydrogenation on Rh catalyst. Therefore, Rh catalyst can lead to lower carbon deposition in the reaction related to CH_4 reaction. In addition, the results of thermodynamic and kinetic also show that CH_4 dehydrogenation on Rh(1 0 0) surface is the most preferable reaction pathway in comparison with those on Rh(1 1 0) and Rh(1 1 1) surfaces.

4. Conclusions

The dehydrogenation of CH_x (x = 1–4) on Rh(1 1 1), Rh(1 1 0) and Rh(1 0 0) surfaces have been systematically investigated by using density functional theory together with periodic slab model. The preferred sites of the adsorbed species are located on the basis of the adsorption energies. On Rh(1 1 1) surface, CH_x (x = 0–3) species and H prefer to adsorb at the three-fold sites. On Rh(1 0 0) surface, the hollow site is preferred for the hydrocarbon groups except CH_3 and H, which prefers to adsorb at the bridge site. On Rh(1 1 0) surface, the preferred sites are different, short-bridge site for CH_3, CH_2 and H, long-bridge site for CH and C. The kinetic results show that on Rh(1 1 1) and Rh(1 0 0) surfaces, CH is the most abundant CH_x species for CH_4 dissociation. On Rh(1 1 0) surface, CH_2 is the most abundant CH_x species. Therefore, our results can give a microscopic reason that why Rh catalyst can lead to lower carbon deposition in the reaction related to CH_4.

Acknowledgments

The authors gratefully acknowledge the financial support of this study by the National Natural Science Foundation of China (Grant Nos. 20906066 and 20976115).

References

[1] W. Huang, K.C. Xie, J.P. Wang, Z.H. Gao, L.H. Yin, Q.M. Zhu, J. Catal. 201 (2001) 100–104.
[2] Y.H. Ding, W. Huang, Y.G. Wang, Fuel Process. Technol. 88 (2007) 319–324.
[3] D.W. Blaylock, T. Ogura, W.H. Green, G.J.O. Beran, J. Phys. Chem. C 113 (2009) 4898–4908.
[4] Y.A. Zhu, D. Chen, X.G. Zhou, W.K. Yuan, Catal. Today 148 (2009) 260–267.
[5] M.F. Haroun, P.S. Moussounda, P. Légaré, J. Mol. Struct. (THEOCHEM) 903 (2009) 83–88.
[6] W. An, X.C. Zeng, C.H. Turner, J. Chem. Phys 131 (2009) 174702-1–174702-11.
[7] S.G. Wang, X.Y. Liao, J. Hu, D.B. Cao, Y.W. Li, J.G. Wang, H.J. Jiao, Surf. Sci. 601 (2007) 1271–1284.
[8] Z.J. Zuo, W. Huang, P.D. Han, Z.H. Li, Appl. Surf. Sci. 256 (2010) 5929–5934.
[9] S.G. Wang, D.B. Cao, Y.W. Li, J.G. Wang, H.J. Jiao, J. Phys. Chem. B 110 (2006) 9976–9983.
[10] J.F. Paul, P. Sautet, J. Phys. Chem. B 102 (1998) 1578–1585.
[11] M.C.J. Bradford, M.A. Vannice, Catal. Rev. Sci. Eng. 41 (1999) 1–42.
[12] C.T. Au, H.Y. Wang, J. Catal. 167 (1997) 337–345.
[13] D.C. Seets, C.T. Reeves, B.A. Ferguson, M.C. Wheeler, C.B. Mullins, J. Chem. Phys. 107 (1997) 10229–10241.
[14] I.M. Ciobîcă, F. Frechard, R.A. van Santen, A.W. Kleyn, J.P.J. Hafner, J. Phys. Chem. B 104 (2000) 3364–3369.
[15] H.L. Abbott, I. Harrison, J. Catal. 254 (2008) 27–38.
[16] C.J. Zhang, P. Hu, J. Chem. Phys. 116 (2002) 322–327.
[17] B.S. Bunnik, G.J. Kramer, J. Catal. 242 (2006) 309–318.
[18] S.G. Wang, D.B. Cao, Y.W. Li, J.G. Wang, H.J. Jiao, Surf. Sci. 600 (2006) 3226–3234.
[19] B.S. Bunnik, G.J. Kramer, R. Santen, Top. Catal. 53 (2010) 403–416.
[20] A. Kokalj, N. Bonini, C. Sbraccia, S. de Gironcoli, S. Baroni, J. Am. Chem. Soc. 126 (2004) 16732–16733.
[21] A. Kokalj, N. Bonini, S. de Gironcoli, C. Sbraccia, G. Fratesi, S. Baroni, J. Am. Chem. Soc. 128 (2006) 12448–12454.
[22] M.S. Liao, Q.E. Zhang, J. Mol. Catal. A: Chem. 136 (1998) 185–194.
[23] C.T. Au, C.F. Ng, M.S. Liao, J. Catal. 185 (1999) 12–22.
[24] C.T. Au, M.S. Liao, C.F. Ng, Chem. Phys. Lett. 267 (1997) 44–50.
[25] H. Burghgraef, A.P.J. Jansen, R.A. van Santen, Surf. Sci. 324 (1995) 345–356.
[26] I.M. Ciobîcă, R.A. van Santen, J. Phys. Chem. B 106 (2002) 6200–6205.
[27] I.M. Ciobîcă, F. Frechard, R.A. van Santen, A.W. Kleyn, J.P.J. Hafner, Chem. Phys. Lett. 311 (1999) 185–192.
[28] Y.M. Choi, P. Liu, J. Am. Chem. Soc. 131 (2009) 13054–13061.
[29] R. Horn, K.A. Williams, N.J. Degenstein, A. Bitsch-Larsen, D. Dalle Nogare, S.A. Tupy, L.D. Schmidt, J. Catal. 249 (2007) 380–393.
[30] T. Yang, X.D. Wen, C.F. Huo, Y.W. Li, J.G. Wang, H.J. Jiao, J. Mol. Catal. A: Chem. 30 (2009) 129–136.
[31] P. Lukinskas, D. Fărcaşiu, Appl. Catal. A: Gen. 209 (2001) 193–205.
[32] M.Y. Sun, A.E. Nelson, J. Adjaye, J. Catal. 233 (2005) 411–421.
[33] M. Pozzo, D. Alfè, Int. J. Hydrogen Energy 34 (2009) 1922–1930.
[34] J. Kua, F. Faglioni, W.A. Goddard, J. Am. Chem. Soc. 122 (2000) 2309–2321.
[35] G. Henkelman, H. Jónnson, Phys. Rev. Lett. 86 (2001) 664–667.
[36] X.Y. Pang, C. Wang, Y.H. Zhou, J.M. Zhao, G.C. Wang, J. Mol. Struct. 948 (2010) 1–10.
[37] Y.A. Zhu, Y.C. Dai, D. Chen, W.K. Yuan, J. Mol. Catal. A: Chem. 264 (2007) 299–308.
[38] A. Michaelides, P. Hu, Surf. Sci. 437 (1999) 362–376.
[39] J.E. Mueller, A.C.T. van Duin, W.A. Goddard, J. Phys. Chem. C 113 (2009) 20290–20306.
[40] Y.A. Zhu, X.G. Zhou, D. Chen, W.K. Yuan, Asia-Pac. J. Chem. Eng. 4 (2009) 511–517.
[41] M. Mavrikakis, J. Rempel, J. Greeley, L.B. Hansen, J.K. Nørskov, J. Chem. Phys. 117 (2002) 6737–6744.
[42] M.M. Yang, X.H. Bao, W.X. Li, J. Chem. Phys 127 (2007) 024705-1–024750-10.
[43] G. Fratesi, S. de Gironcoli, J. Chem. Phys. 125 (2006) 044701-1–044701-7.
[44] P.W. van Grootel, E.J.M. Hensen, R.A. van Santen, Langmuir 26 (2010) 16339–16348.
[45] J. Chen, Z.P. Liu, J. Am. Chem. Soc. 130 (2008) 7929–7937.
[46] T. Koerts, R.A. van Santen, J. Mol. Catal. 70 (1991) 119–127.
[47] F. Solymosi, Catal. Today 28 (1996) 193–203.
[48] H.Y. Xiao, D.Q. Xie, Surf. Sci. 558 (2004) 15–22.
[49] M.D. Segall, P.J.D. Lindan, M.J. Probert, C.J. Pickard, P.J. Hasnip, S.J. Clark, M.C. Payne, J. Phys. Condens. Matter 14 (2002) 2717–2744.
[50] J.P. Perdew, A. Zunger, Phys. Rev. B 23 (1981) 5048–5079.
[51] J.P. Perdew, J.A. Chevary, S.H. Vosko, K.A. Jackson, M.R. Pederson, D.J. Singh, C. Fiolhais, Phys. Rev. B 46 (1992) 6671–6687.
[52] D. Vanderbilt, Phys. Rev. B 41 (1990) 7892–7895.
[53] O.R. Inderwildi, S.J. Jenkins, D.A. King, J. Am. Chem. Soc. 129 (2007) 1751–1759.
[54] J.W. Medlin, M.D. Allendorf, J. Phys. Chem. B 107 (2003) 217–223.
[55] T.A. Halgren, W.N. Lipscomb, Chem. Phys. Lett. 49 (1977) 225–232.
[56] D.R. Lide (Ed.), CRC Handbook of Chemistry and Physics, 67th ed., CRC, Boca Raton, FL, 1983.
[57] C.S. Barrett, T.B. Massalski, Structure of Metals, McGraw-Hill, New York, 1966.
[58] R. He, H. Kusaka, M. Mavrikakis, J.A. Dumesic, J. Catal. 217 (2003) 209–221.
[59] J.M.H. Lo, T. Ziegler, J. Phys. Chem. C 112 (2008) 13642–13649.
[60] J. Kiss, A. Kis, F. Solymosi, Surf. Sci. 454–456 (2000) 273–279.
[61] E.J. Walter, A.M. Rappe, Surf. Sci. 549 (2004) 265–272.
[62] A. de Koster, R.A. van Santen, Surf. Sci. 233 (1990) 366–380.
[63] M.J.P. Hopstaken, J.W. Niemantsverdriet, J. Phys. Chem. B 104 (2000) 3058–3066.
[64] X.C. Fu, W.X. Shen, T.Y. Yao, Physical Chemistry, 4th ed., Higher Education Press, Beijing, 1990.